

Dispersion in rectangular networks: effective diffusivity and large-deviation rate function

Alexandra Tzella¹ and Jacques Vanneste²

¹*School of Mathematics, University of Birmingham, United Kingdom*

²*School of Mathematics and Maxwell Institute for Mathematical Sciences, University of Edinburgh, United Kingdom*
(Dated: May 26, 2022)

We investigate the dispersion of a passive scalar released in a fluid flowing within a rectangular, Manhattan-style network. We use large-deviation theory to approximate the scalar concentration as it evolves under the combined action of advection and diffusion and derive an expression for the rate function that controls the form of the concentration at large times t . For moderately large distances $O(t^{1/2})$ from the centre of mass, this form reduces to a Gaussian parameterised by a (tensorial) effective diffusivity given in closed form. Further away, at distances $O(t)$, a more complex form reveals the strong imprint of the network geometry. Our theoretical predictions are verified against Monte Carlo simulations of Brownian particles.

PACS numbers: 05.40.-a, 05.60.Cd, 47.51.+a, 47.56.+r, 47.85.lk

The dispersion of passive scalars in fluid flows is of paramount importance in many areas of science and engineering. At its heart lies a subtle interplay between flow advection and molecular diffusion as originally identified by Taylor [1]. The picture is more complex still when the flow is constrained within a non-trivial geometry such as that of a network. Dispersion on networks has many applications: vascular and respiratory flows [2], porous media [3–5], urban networks [6], etc. In these applications, the focus is often on the spatial spreading of a scalar released in the network at an initial time. After some time, the scalar concentration typically takes a Gaussian form, characterised by the speed of the centre of mass and an effective diffusivity tensor. In simple geometries, e.g. periodic networks, these parameters can be computed using the method of homogenisation [7–10] or the method of moments [11, 12]. The Gaussian form captures the core of the scalar distribution (specifically for distances $O(t^{1/2})$ away from the centre of mass) but not its tails which are not universal. Capturing these requires to apply the more sophisticated theory of large deviations [13, 14]. This applies to $O(t)$ distances and predicts a scalar concentration of the form $\exp(-tg(x/t))$, where g is a rate function [15].

Here, we compute g for the simplest network, namely the rectangular network illustrated in Fig. 1. This consists of a rectangular array of one-dimensional edges of length L in the x -direction and βL in the y -direction in which fluid flows with uniform velocity (U, V) . The rate function is found as the Legendre transform of the solution of an explicit transcendental equation; its form, especially in asymptotic limits, sheds light on the rich interaction between advection, diffusion and geometry in this problem. A quadratic approximation of g near its minimum provides useful closed-form expressions for the effective diffusivity tensor which we have been unable to find in the literature.

Model.—Taking L as reference length and the diffusive

time scale L^2/κ as reference time, the advection–diffusion equations for the scalar concentration C read

$$\partial_t C + U \partial_x C = \partial_{xx}^2 C \quad \text{and} \quad \partial_t C + V \partial_y C = \partial_{yy}^2 C, \quad (1)$$

in edges oriented in the x - and y -directions [16]. The non-dimensional parameters U and V are Péclet numbers measuring the strength of advection relative to diffusion. These equations are supplemented by boundary conditions applied at the vertices separated by distances 1 in x and β in y . The boundary conditions express (i) continuity of C ,

$$C|_W = C|_E = C|_S = C|_N, \quad (2)$$

where the subscripts denote the limiting value to the west, east, etc. of the vertex, and (ii) vanishing of the net concentration flux which, on using (2), simplifies into

$$\partial_x C|_W + \partial_y C|_S = \partial_x C|_E + \partial_y C|_N. \quad (3)$$

Eqs. (1)–(3) form a closed system which can be solved to predict the evolution of C for arbitrary initial conditions (e.g. numerically, using Laplace transform [17, 18]). Here we consider a scalar that is initially released at a vertex taken to be the origin so that $C(x, y, 0) = \delta(x)\delta(y)$.

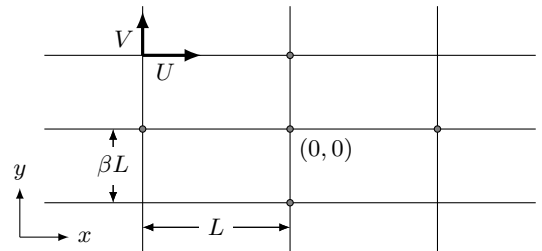


FIG. 1. A section of the rectangular network which includes the vertex at $(x, y) = (0, 0)$. Fluid flows with velocity (U, V) along edges of length L and βL , respectively.

Large deviations.—Analytic progress is possible using the theory of large deviations [13, 14]. This describes the concentration in the long-time limit $t \gg 1$ as [15]

$$C \sim t^{-1} \phi(x, y) e^{-tg(\boldsymbol{\xi})}, \quad \text{with } \boldsymbol{\xi} = (x, y)/t. \quad (4)$$

The rate (or Cramér) function $g(\boldsymbol{\xi})$, thought of as continuous with $\boldsymbol{\xi} \in \mathbb{R}^2$, describes the most rapid changes in C and is the main object of interest. The function ϕ is supported on the network and has periods 1 and β in x and y . The factor t^{-1} is imposed by normalisation. Introducing (4) into (1) leads to

$$\partial_{xx}\phi - (U + 2q_x)\partial_x\phi + (Uq_x + q_x^2)\phi = f(\mathbf{q})\phi, \quad (5)$$

$$\partial_{yy}\phi - (V + 2q_y)\partial_y\phi + (Vq_y + q_y^2)\phi = f(\mathbf{q})\phi. \quad (6)$$

To write these we have defined

$$\mathbf{q} = (q_x, q_y)^T = \nabla g \quad \text{and} \quad f(\mathbf{q}) = \boldsymbol{\xi} \cdot \mathbf{q} - g(\boldsymbol{\xi}), \quad (7)$$

which implies that f and g are Legendre transforms of one another, with \mathbf{q} and $\boldsymbol{\xi}$ the dual independent variables. Eqs. (5)–(6) are supplemented by the boundary conditions inferred from (2) and (3): continuity of ϕ and

$$\partial_x\phi|_W + \partial_y\phi|_S = \partial_x\phi|_E + \partial_y\phi|_N. \quad (8)$$

Together, (5)–(8) form a family of eigenvalue problems parameterized by \mathbf{q} , with $f(\mathbf{q})$ as the eigenvalue and ϕ as the eigenfunction.

We now solve (5)–(8) explicitly. Consider the vertex at $(x, y) = (0, 0)$ and denote by $\phi_E(x)$ the eigenfunction in the edge to the east of it, and by A the value of ϕ at the vertex $(0, 0)$ and hence, by periodicity, at all vertices. Solving (5) with the boundary conditions $\phi_E(0) = \phi_E(1) = A$, we find that

$$\phi_E(x) = \frac{A}{\sinh \alpha_U} \left(e^{(q_x + U/2)x} \sinh(\alpha_U(1-x)) + e^{(q_x + U/2)(x-1)} \sinh(\alpha_U x) \right), \quad (9)$$

where $\alpha_U = \sqrt{f(\mathbf{q}) + U^2/4}$. By periodicity, the solution to the west of $(0, 0)$ is $\phi_W(x) = \phi_E(x+1)$. Similarly, the solution ϕ_N to the north is found by solving (6) with $\phi_N(0) = \phi_N(\beta) = A$ which yields

$$\phi_N(y) = \frac{A}{\sinh(\alpha_V\beta)} \left(e^{(q_y + V/2)y} \sinh(\alpha_V(\beta-y)) + e^{(q_y + V/2)(y-\beta)} \sinh(\alpha_V y) \right), \quad (10)$$

where $\alpha_V = \sqrt{f(\mathbf{q}) + V^2/4}$. The solution to the south is $\phi_S(y) = \phi_N(y+\beta)$.

Introducing (9)–(10) into (8) gives

$$\frac{\alpha_U \cosh \alpha_U}{\sinh \alpha_U} + \frac{\alpha_V \cosh(\alpha_V \beta)}{\sinh(\alpha_V \beta)} = \frac{\alpha_U \cosh(q_x + U/2)}{\sinh \alpha_U} + \frac{\alpha_V \cosh((q_y + V/2)\beta)}{\sinh(\alpha_V \beta)}. \quad (11)$$

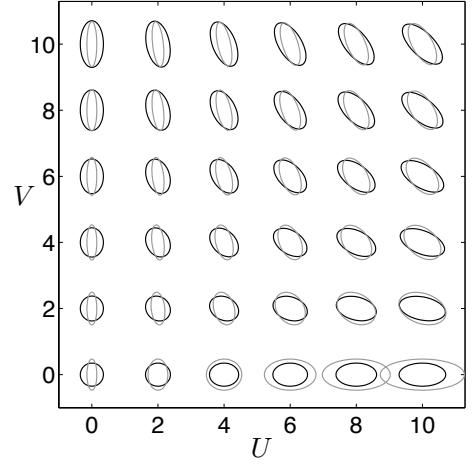


FIG. 2. Ellipses of constant $\mathbf{x}^T \mathbf{K}^{-1} \mathbf{x}$ representing the effective diffusivity tensor \mathbf{K} as a function of U and V for $\beta = 1$ (black) and $\beta = 10$ (grey).

This transcendental equation for $f(\mathbf{q})$ (recall that $f(\mathbf{q})$ appears in α_U and α_V) is our central result. It can be solved numerically for a range of \mathbf{q} to obtain $f(\mathbf{q})$; the rate function $g(\boldsymbol{\xi})$ is deduced by taking the Legendre transform. We start our analysis by considering the small- \mathbf{q} behaviour of $f(\mathbf{q})$ which provides closed-form expressions for the effective diffusivity of the network.

Effective diffusivity.—Taylor-expanding $f(\mathbf{q})$ around $\mathbf{q} = 0$ and using that $f(\mathbf{0}) = 0$, we write

$$f(\mathbf{q}) = \boldsymbol{\xi}_* \cdot \mathbf{q} + \frac{1}{2} \mathbf{q}^T \mathbf{H}_f \mathbf{q} + o(|\mathbf{q}|^2), \quad (12)$$

where $\boldsymbol{\xi}_* = \nabla f(\mathbf{0})$ and \mathbf{H}_f is the Hessian of f at $\mathbf{q} = 0$ [15]. Taking the Legendre transform, yields a quadratic approximation to g valid for $|\boldsymbol{\xi} - \boldsymbol{\xi}_*| \ll 1$. This reduces (4) to the Gaussian, diffusive approximation

$$C(\mathbf{x}, t) \sim e^{-(\mathbf{x} - \boldsymbol{\xi}_* t)^T \mathbf{K}^{-1} (\mathbf{x} - \boldsymbol{\xi}_* t) / (4t)}, \quad (13)$$

where $\boldsymbol{\xi}_*$ is the velocity of the centre of mass of the scalar and $\mathbf{K} = \mathbf{H}_f/2$ is the effective diffusivity tensor. Note that effective diffusivities are more commonly derived using the method of homogenization [7–10] or the method of moments [11, 12]: solving their cell problem amounts to the perturbative solution of (5)–(8) [15]. Expanding (11) for small f and \mathbf{q} and solving for f gives, after considerable manipulations best carried out with a computer-algebra package, the velocity

$$\boldsymbol{\xi}_* = \left(\frac{U}{1+\beta}, \frac{\beta V}{1+\beta} \right) \quad (14)$$

and the components of the effective diffusivity tensor

$$K_{11} = \frac{(1 + \beta)^2 + \beta^2 U^2 (h(U) + \beta h(\beta V))}{(1 + \beta)^3}, \quad (15)$$

$$K_{22} = \frac{\beta(1 + \beta)^2 + \beta^2 V^2 (h(U) + \beta h(\beta V))}{(1 + \beta)^3}, \quad (16)$$

$$K_{12} = K_{21} = -\frac{\beta^2 UV (h(U) + \beta h(\beta V))}{(1 + \beta)^3}, \quad (17)$$

where we have defined $h(x) = x^{-2}(x \coth(x/2)/2 - 1)$.

These explicit expressions illustrate the complex interplay between advection and diffusion that determines the dispersive property of the network. They are visualised for a range of U and V and two values of β as ellipses of constant $\mathbf{x}^T \mathbf{K}^{-1} \mathbf{x}$ (corresponding to constant concentration) in Fig. 2. For small U and V (small Péclet number), the asymptotic formula $h(x) = 1/12 + O(x^2)$ as $x \rightarrow 0$ provides the approximation $K_{11} \sim 1/(1 + \beta) + \gamma U^2$, $K_{22} \sim \beta/(1 + \beta) + \gamma V^2$ and $K_{12} \sim -\gamma UV$, with $\gamma = \beta^2/(12(1 + \beta)^2)$. The leading-order, Péclet-independent terms can be interpreted by noting that, because of the $1 : \beta$ ratio of the edge lengths, particles diffuse in x for a fraction $1/(1 + \beta)$ of the time and in y for a fraction $\beta/(1 + \beta)$. Because γ is numerically small, the $O(U^2, V^2)$ corrections associated with advection are particularly weak (see bottom left of Fig. 2).

For large U and V (large Péclet number), we use $h(x) = 1/(2x) + O(x^{-2})$ as $x \rightarrow \infty$ to approximate the effective diffusivity components as $K_{11} \sim \delta U^2$, $K_{22} \sim \delta V^2$ and $K_{12} \sim -\delta UV$, with $\delta = \beta^2(U^{-1} + V^{-1})/(2(1 + \beta)^3)$. These grow linearly in U and V which dimensionally corresponds to components that scale like LU^* , where U^* is the characteristic speed, and are independent of the molecular diffusivity κ . This is characteristic of a regime termed geometric dispersion [19] or mechanical dispersion in the porous media literature [5, 20]. Note that the tensor \mathbf{K} is singular to leading order in U and V : effective diffusion is strong in the direction $(-U, V)$ but weak in the perpendicular direction (V, U) (see top right of Fig. 2). Note also that the large- (U, V) approximation of \mathbf{K} can be recovered by a spatially discrete random-walk model in which particles move purely advectively along the edges, selecting between the two outward-flowing edges with probability $p = U/(U + V)$ in the x -direction and $1 - p$ in the y -direction [21]. This generalises results obtained by [22] in the case $p = 1/2$.

Rate function.—Effective diffusivity provides only a partial description of dispersion: the rate function g obtained from (11) is much more informative. This is demonstrated in Fig. 3 which shows typical examples of g obtained numerically for two values of (U, V) (for $\beta = 1$) and its quadratic approximation corresponding to the Gaussian (13). This quadratic approximation is excellent in the vicinity of ξ_* , with circular (Fig. 3(a)) and elliptical contours (Fig. 3(b)). Beyond the vicinity of ξ_* , it is inadequate, failing for instance to capture the

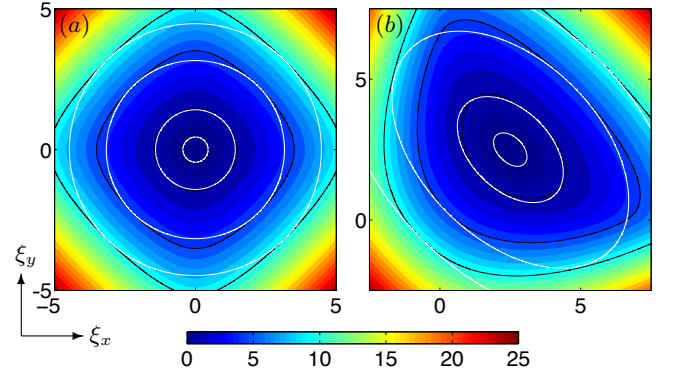


FIG. 3. (Color online.) Rate function g calculated numerically from (11) for $\beta = 1$ and (a) $(U, V) = (0, 0)$ and (b) $(5, 5)$. Selected contours (with values 0.1, 1, 5 and 10) compare g (black) with its quadratic approximation (white) corresponding to the Gaussian approximation (13). This approximation is clearly valid near the minimum ξ_* of g .

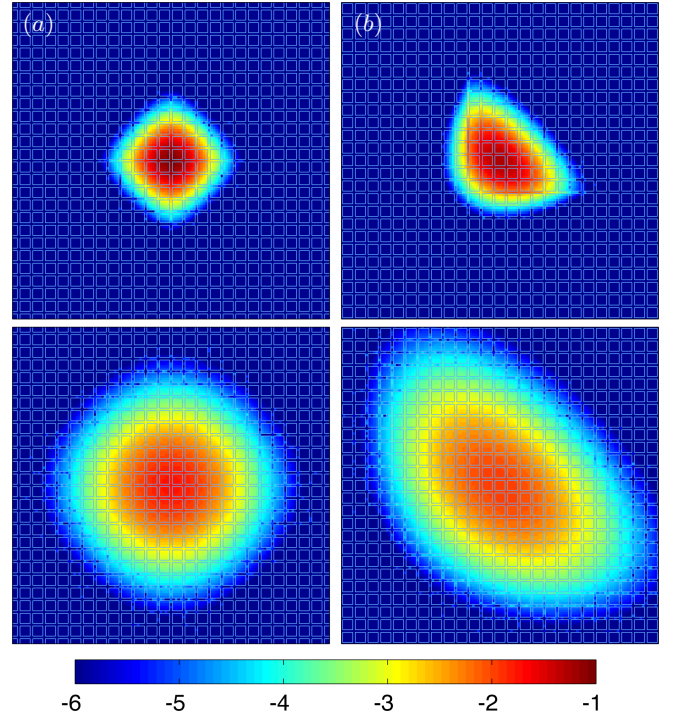


FIG. 4. (Color online.) Snapshots of $\log_{10} C$ for $t = 1$ (top) and $t = 5$ (bottom) for the parameters of Fig. 3. Numerical results are shown inside the network (the edges' width is made finite for visual purpose). The large-deviation prediction (4) and (11) is shown outside the network.

anisotropy of g and hence of C for $U = V = 0$, or underestimating g in large portions of the ξ -plane (hence overestimating C by an exponentially large factor) for $U = V \neq 0$. Note however that for $U = V$ and $\beta = 1$, f is exactly quadratic along the line $q_x = q_y$ (see (11)); as a result, g coincides with its quadratic approximation

for $\xi_x = \xi_y$ as is evident in Fig. 3.

The limitations of the quadratic (Gaussian) approximation are best demonstrated by considering the large- ξ behaviour of $g(\xi)$ or, equivalently, the large- q behaviour of $f(q)$. In this regime, and with the distinguished scaling $U, V = O(|q|)$, (11) reduces to

$$\alpha_U + \alpha_V \sim \alpha_U \cosh(q_x + U/2)e^{-\alpha_V} + \alpha_V \cosh(\beta(q_y + V/2))e^{-\beta\alpha_V}. \quad (18)$$

Either term on the right-hand side is exponentially large, precluding the solution of (18) unless

$$f(q) \sim \max(q_x^2 + Uq_x, q_y^2 + Vq_y). \quad (19)$$

This gives a leading-order approximation to f which, remarkably, is independent of β . The Legendre transform of (19) is cumbersome for arbitrary U and V , but physical insight is gained by considering limiting cases. For $U = V = 0$, (19) leads to $g(\xi) \sim (|\xi_x| + |\xi_y|)^2/4$, in accordance with the diamond-shaped contours of g for large ξ in Fig. 3(a). This implies a concentration $C \sim \exp(-(|x| + |y|)^2/(4t))$, which can be interpreted as resulting from a generalised form of diffusion where the Euclidian distance is replaced by the L^1 (or Manhattan) distance. In the opposite limit where Uq_x and Vq_y dominate q_x^2 and q_y^2 in (19), the linear dependence of f on q implies that $g \rightarrow \infty$ as $\xi_x \rightarrow U$ and as $\xi_y \rightarrow V$, reflecting the finite propagation speed of the scalar when molecular diffusion is neglected against advection.

The large-Péclet regime $U, V \gg 1$ (and $\xi = O(1)$) is of interest. In this regime, $f = O(U, V)$ and (11) becomes

$$U(e^{q_x - f/U} - 1) + V(e^{q_y - f/V} - 1) = 0. \quad (20)$$

While this equation does not appear to have an analytic solution, it can be used to show that the concentration has a dimensional form that is independent of molecular diffusivity, generalising the notion of geometric or mechanical dispersion to the large-deviation regime.

Monte Carlo simulations.—We now test our predictions against Monte Carlo simulations of Brownian particles. The concentration, derived as the PDF of their positions $\mathbf{X}(t)$, is compared with the large-deviation estimate in Fig. 4. The PDF is obtained from an ensemble of $N = 10^6$ particles by integrating the stochastic differential equations associated with (1), with the additional microscopic rule that particles entering a vertex exit through a random edge. The large-deviation approximation (4) is seen to provide an excellent approximation to the concentration. Although formally valid for $t \gg 1$, it is remarkably accurate for the moderate values of $t = 1$ and 5 considered. The relevance of the large-deviation approximation is clear at $t = 1$, when comparing Figs. 3 and 4. As time progresses, the Gaussian approximation (13) becomes sufficient to describe the bulk of the scalar

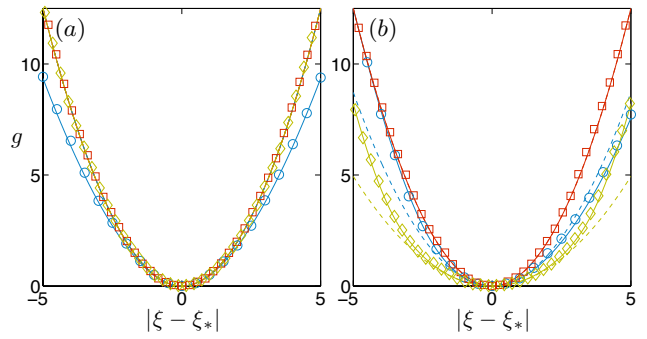


FIG. 5. (Color online.) Cross sections of the rate function g for the parameters of Fig. 3. The large-deviation and Gaussian predictions (solid and dashed lines) are compared with Monte Carlo results (symbols) as a function of $|\xi - \xi_*|$ in the directions (1,0) (\circ), (1,1) (\square) and (1,-1) (\diamond). Because $U = V$, the Gaussian and large-deviation predictions coincide in the direction (1,1) (and in direction (1,-1) in panel (a)).

patch which assumes the elliptical form characteristic of the Gaussian regime (cf. Fig. 3).

A detailed assessment of the large-deviation approximation requires a careful numerical evaluation of the rate function g . This is achieved by estimating its Legendre transform as the scaled cumulant generating function [23–25] $f(q) = \lim_{t \rightarrow \infty} t^{-1} \log \mathbb{E} e^{q \cdot \mathbf{X}(t)}$, where the expectation \mathbb{E} over the Brownian motion is estimated by a Monte Carlo procedure. To reduce sampling error to an acceptable level, we have adopted the importance-sampling technique described in [15], based on the pruning-cloning technique of [26]. Fig. 5 shows an excellent agreement between large-deviation predictions and numerical results (obtained from an ensemble of $N = 10^3$ particles at $t = 5$) and illustrates the restricted range of validity of the Gaussian approximation.

Conclusion.—This paper considers the long-time dispersive properties of a rectangular network using large-deviation theory. The rate function g , shown to satisfy the explicit equation (11), describes the scalar concentration over a broad range of scales $|\mathbf{x} - \xi_* t| = O(t)$. In the narrower range $|\mathbf{x} - \xi_* t| = O(t^{1/2})$, it recovers the Gaussian, diffusive approximation and provides a convenient route for the derivation of the corresponding effective diffusivity. The results highlight the role of the network geometry and the finiteness of the advection speed in determining the concentration well away from the centre of mass. They are directly applicable to determine the speed of a class of reactive fronts which is closely linked to g [14, 27]. The approach employed clearly generalises to other periodic networks, as we will describe elsewhere. Other useful generalisations include networks composed of edges with finite cross sections (pipes, channels), leaky networks and random networks (see [3, 17–19, 28–30] and references therein).

The work was supported by EPSRC (Grant No. EP/I028072/1).

-
- [1] G. I. Taylor, Proc. R. Soc. Lond. A **219**, 186 (1953).
- [2] G. A. Truskey, F. Yuan, and D. F. Katz, *Transport Phenomena in Biological Systems* (Pearson Prentice Hall, 2004).
- [3] P. M. Adler, *Porous Media: Geometry and Transports* (Butterworth/Heinemann, Boston, 1992).
- [4] H. Brenner and D. A. Edwards, *Macrotransport Processes* (Butterworth/Heinemann, Boston, 1993).
- [5] M. Sahimi, Rev. Mod. Phys. **65**, 1393 (1993).
- [6] S. E. Belcher, Philos. T. Roy. Soc. A **363**, 2947 (2005).
- [7] A. A. Bensoussan, J. L. Lions, and G. Papanicolaou, *Asymptotic analysis for periodic structures* (North Holland, 1978).
- [8] J. Rubinstein and R. Mauri, SIAM J. Appl. Math. **46**, pp. 1018 (1986).
- [9] C. Mei, Transport Porous Med. **9**, 261 (1992).
- [10] J. Auriault and P. Adler, Adv. Water Resour. **18**, 217 (1995).
- [11] R. Aris, Proc. R. Soc. Lond. A **235**, 67 (1956).
- [12] H. Brenner, Proc. R. Soc. Lond. A **297**, 81 (1980).
- [13] M. I. Friedlin and A. D. Wentzell, *Random Perturbations of Dynamical Systems* (Springer-Verlag, New York, 1984).
- [14] M. Friedlin, *Functional Integration and Partial Differential Equations* (Princeton University Press, Princeton, 1985).
- [15] P. H. Haynes and J. Vanneste, J. Fluid Mech. **745**, 321 (2014).
- [16] For pipe flows, (U, V) can be interpreted as a section-averaged velocity and κ as a Taylor diffusivity.
- [17] L. de Arcangelis, J. Koplik, S. Redner, and D. Wilkinson, Phys. Rev. Lett. **57**, 996 (1986).
- [18] L. L. M. Heaton, E. López, P. K. Maini, M. D. Fricker, and N. S. Jones, Phys. Rev. E **86**, 021905 (2012).
- [19] J.-P. Bouchaud and A. Georges, Phys. Rep. **195**, 127 (1990).
- [20] D. L. Koch and J. F. Brady, J. Fluid Mech. **154**, 399 (1985).
- [21] The same effective microscopic rule is obtained in [17] by considering transport around a single vertex.
- [22] S. E. Belcher, O. Coceal, E. V. Goulart, A. C. Rudd, and A. G. Robins, J. Fluid Mech. **763**, 51 (2015).
- [23] R. S. Ellis, Actuarial J. **1**, 97 (1995).
- [24] A. Dembo and O. Zeitouni, *Large deviations: techniques and applications*, Application of Mathematics, Vol. 38 (Springer-Verlag, New York, 1998).
- [25] H. Touchette, Phys. Rep. **478**, 1 (2009).
- [26] P. Grassberger, Phys. Rev. E **56**, 3682 (1997).
- [27] A. Tzella and J. Vanneste, SIAM J. Appl. Math. **75**, 1789 (2015).
- [28] J. Koplik, S. Redner, and D. Wilkinson, Phys. Rev. A **37**, 2619 (1988).
- [29] D. ben Avraham and S. Havlin, *Diffusion and Reactions in Fractals and Disordered Systems* (Cambridge University Press, New York, 2000).
- [30] P. K. Kang, M. Dentz, T. Le Borgne, and R. Juanes, Phys. Rev. Lett. **107**, 180602 (2011).